AD_____

Award Number: W81XWH-13-1-0064

TITLE: A Structural Biology and Protein Engineering Approach to the Development of Antidotes against the Inhibition of Human Acetylcholinesterase by OP-based Nerve Agents

PRINCIPAL INVESTIGATOR: Joel L. Sussman

CONTRACTING ORGANIZATION: Weizmann Institute of Science
Rehovot 76100 ISRAEL

REPORT DATE: May 2015

TYPE OF REPORT: Final

PREPARED FOR: U.S. Army Medical Research and Materiel Command
Fort Detrick, Maryland 21702-5012

REPORT DOCUMENTATION PAGE

Form Approved
OMB No. 0704-0188

1. REPORT DATE	2. REPORT TYPE	3. DATES COVERED
May 2015	Final	11 Feb 2013 - 10 Feb 2015

4. TITLE AND SUBTITLE
A Structural Biology and Protein Engineering Approach to the Development of Antidotes against the Inhibition of Human Acetylcholinesterase by OP-based Nerve Agents

5a. CONTRACT NUMBER

5b. GRANT NUMBER
W81XWH-13-1-0064

5c. PROGRAM ELEMENT NUMBER

6. AUTHOR(S)
Joel L. Sussman – PI
Dan S. Tawfik – Co PI

E-Mail: Joel.Sussman@weizmann.ac.il

5d. PROJECT NUMBER

5e. TASK NUMBER

5f. WORK UNIT NUMBER

7. PERFORMING ORGANIZATION NAME(S) AND ADDRESS(ES)
Weizmann Institute of Science
Rehovot 76100 ISRAEL

8. PERFORMING ORGANIZATION REPORT NUMBER

9. SPONSORING / MONITORING AGENCY NAME(S) AND ADDRESS(ES)
U.S. Army Medical Research and Materiel Command
Fort Detrick, Maryland 21702-5012

10. SPONSOR/MONITOR'S ACRONYM(S)

11. SPONSOR/MONITOR'S REPORT NUMBER(S)

12. DISTRIBUTION / AVAILABILITY STATEMENT
Approved for Public Release; Distribution Unlimited

13. SUPPLEMENTARY NOTES

14. ABSTRACT

The human acetylcholinesterase (hAChE) gene was cloned into the pHLsec expression vector. The recombinant enzyme (rhAChEmD) was expressed on a large scale in adherent 293T cells. It was secreted as a monomeric species, purified by affinity chromatography, and deglycosylated with PNGase F. A crystallization screen, using the Mosquito crystallization robot, identified conditions for formation of diffraction-quality crystals in 0.025% dichloromethane/12% PEG 20,000/0.1M imidazole, pH 7.0. The crystals formed in the hexagonal space group $P3_112$, with cell constants a=125.31, b=125.31, c=131.40 Å, and one monomer per asymmetric unit. A complete data set, to 2.9 Å resolution, was collected at 100 K at the ESRF (Grenoble, France). The structure was solved by molecular replacement, resulting in an R_{free} of 23.74%, and R_{work} of 19.31%, for all data to 2.9 Å. The coordinates and structures factors have been deposited in the PDB, with IDcode 4PQE. As an initial step for synthesis of a GF surrogate, the chloridate, $CH_3P(O)(O\text{-cyclohexyl})Cl$, has been synthesized, and will be reacted with coumarin. Synthesis of the pure chiral forms of the coumarin surrogate of VX, both the toxic S_p isomer, and the much less reactive and less toxic R_p form, in accordance with our published protocol, permitted preparation of the corresponding crystalline OP/hAChE conjugates using the hAChE expressed in HEK293 cells, purified by affinity chromatography, and deglycosylated so as to produce well-diffracting crystals. The crystal structure of the R_p conjugate has been solved to 2.7 Å, and reveals the interactions of the atoms of the OP moiety with amino-acid side-chains at atomic resolution. Conditions have also been developed for expression of a full-length rhAChE construct, $rhAChE_T$, which assembles to form the physiological tetramer.

15. SUBJECT TERMS
human acetylcholinesterase; cloning; expression; X-ray structure; 3D structure; chemical synthesis; GF surrogate

16. SECURITY CLASSIFICATION OF:			17. LIMITATION OF ABSTRACT	18. NUMBER OF PAGES	19a. NAME OF RESPONSIBLE PERSON
a. REPORT	b. ABSTRACT	c. THIS PAGE			USAMRMC
U	U	U	UU	30	19b. TELEPHONE NUMBER *(include area code)*

TABLE OF CONTENTS

1. INTRODUCTION

Human acetylcholinesterase (hAChE) is the primary target of organophosphorus (OP) nerve agents. Despite the great importance of the crystal structure of native human AChE (hAChE) for development of countermeasures against OP-based nerve agents and pesticides, as well as for other pharmacological applications, such a structure was reported only recently by us (Dvir *et al* [2010] *Chem-Biol Interact* **187**:10-22) and subsequently by Cheung (Cheung et al [2012] *J Med Chem* **55**:10282-10286). hAChE crystal structures that we reported earlier (Kryger et al [2000] *Acta Crystallogr D Biol Crystallogr* **56**:1385-1394) were of complexes with the snake venom polypeptide toxin, fasciculin, whose presence would obviously prejudice structure-function studies involving nerve agents and other ligands. Studies on the structures of complexes of hAChE with appropriate oximes, and of conjugates with relevant nerve agents in both their reactivatable and 'aged' forms, will provide crucial information for the design of more effective antidotes in both a prophylactic and a therapeutic context. Such antidotes include:

(1) Inhibitors, such as the carbamate, pyridostigimine, which react with the active site serine of AChE reversibly, and thus shield the enzyme against irreversible inactivation by the nerve agent.

(2) Reactivators, such as oximes, that cleave the covalent phosphoryl-AChE conjugate, thus regenerating the free enzyme.

(3) A combination of exogenously administered engineered AChE and a reactivating oxime reactivator that turns over the phosphonylated scavenger, thus converting it from a stoichiometric to a pseudo-catalytic scavenger.

An additional major benefit of the structural information provided by this research will be to obtain one or more products, based on a combination of hAChE with one or more oxime reactivators that, together, will be capable of pseudocatalytic hydrolysis of all V- or G-agents. It is envisaged that these products will be utilized either prophylactically or in a post-treatment context. Embedded in a suitable medical doctrine they will expedite the recovery and return to full battle capability of the war-fighter. The approach adopted should substantially reduce the amount of the enzyme protein required to afford protection, thus making its availability more economically feasible. In parallel, the civilian population may be exposed to OP nerve agents both in military and terrorist scenarios. Moreover, civilians are quite routinely exposed to, and susceptible to, a variety of commercially available OP-based and carbamate-based insecticides. The same considerations outlined above may also apply to treatment of civilians. The issue of reduced protein dosage, resulting in enhanced cost effectiveness, will be particularly relevant to the civilian arena, where treatment will be administered to a heterogeneous population in terms of age and medical background.

2. BODY

Overexpression of rhAChE in human embryonic kidney cells, H293T

The rhAChE construct used in this study, which encodes residues 32-574 of the mature monomer (Velan *et al* [1991] *Cell Mol Neurobiol* **11:**143-156), was cloned into the pHLsec expression vector. It includes the vector secretion signal followed by the coding sequence of all 543 amino acids of the mature protein (Fig. 1). Transient transfected cells were grown in serum-free medium, and medium containing the secreted protein, rhAChEmD (from which the secretion sequence had been cleaved) was collected 3 and 6 days post transfection.

Purification and deglycosylation of rhAChEmD

Following centrifugation and filtration, the rhAChEmD was purified by affinity chromatography, and then deglycosylated with PNGase F. Basically, this involved affinity purification of the soluble enzyme secreted by the H293T cell cultures, on a Sepharose column to which a quaternary ammonium moiety had been covalently linked via a suitable spacer. The bound rhAChE was displaced from the column by the quaternary ligand, tetramethylammonium bromide, and eluted as a highly purified preparation. In order to enhance the likelihood of obtaining high quality crystals, diffracting to high resolution, the purified enzyme was, as before, treated with the glycosidase, PNGase F (expressed and purified 'in-house' as a GST-PNGase F fusion protein), which removes the entire oligoglycoside chains by cleaving the amide bond by which they are attached to an asparagine residue within the protein sequence.

The preparation used to obtain the crystals was obtained from two 2.5 liter batches of supernatant that were generated sequentially. The first supernatant was collected after 3 days, and the second after 5 days. Each of these supernatants was purified separately, using the same affinity column. Since we did not detect any differences in the degree of purity of the eluted enzyme, or in any other characteristics, they were pooled, dialysed against PBS, and concentrated in an Amicon Ultracell device equipped with a MWCO-30K filter. This procedure yielded 3.5 mg of rhAChE in 4 ml of buffered PBS.

The entire concentrated batch was deglycosylated by incubation with GST-PNGase F at a rhAChEmD/PNGase protein ratio of ~23:1. After incubation for 70 h at 26°C, in the presence of 0.02% NaN_3, the GST-PNGase F was removed by addition of 400 µl of Glutathione Sepharose 4 Fast Flow. After incubation at room temperature for 2 h, the beads were spun down at 3,000 g for 10 min. The supernatant was dialyzed overnight against 100 mM NaCl/1 mM MES, pH 6.5. SDS-PAGE revealed a significant decrease in the molecular weight of the polypeptide, as well as a decrease in intensity of glycostaining.

Concentration of the deglycosylated rhAChEmD was performed in two steps. First, it was concentrated to 1 ml, using an Amicon Ultracell device as described above. It was then further concentrated in a Vivaspin 500 Centrifugal Concentrator, equipped with a

MWCO 30 kD filter, to a final volume of 240 µl, and a final protein concentration of 11 mg/ml.

In addition to the methods of characterization previously used, we now made use of isoelectric focusing (IEF) to compare the purified rhAChE before and after deglycosylation, as shown in Fig. 2. It can be seen, by comparison of lane #7 with lane #2, that deglycosylation modifies the pattern of isoforms, with one band becoming predominant.

Stereospecific synthesis of EMP-CHMC

The details of the stereospecific synthesis of EMP-CHMC (the *O*-ethylmethylphosphonyl ester of cyanohydroxymethylcoumarin), to yield both racemic EMP-CHMC and the resolved chiral forms, [+]-EMP and [-]-EMP, are displayed schematically in Fig. 3.

Crystal structure analysis

Apo rhAChEmD structure

The concentrated solution of rhAChEmD was subjected to a series of crystallization screens, via the sitting drop method, using the Mosquito crystallization robot. Diffraction-quality crystals were obtained from 0.025% dichloromethane/12% PEG 20,000/0.1M imidazole, pH7.0.

The crystals formed in the hexagonal space group $P3_112$, with cell constants a = 125.31, b = 125.31, c = 131.40 Å, and with one monomer per asymmetric unit (Figs. 4 and 5). A complete dataset, to 2.9 Å resolution, was collected at 100 K, from a single crystal, at a wavelength of 0.8726 Å, on beam line ID23-2 at the European Synchrotron Radiation Facility (ESRF) in Grenoble, France. The diffraction images were indexed and integrated using the HKL2000 program (Otwinowski & Minor [1997] *Methods Enzymol* **276:**307-326), and the integrated reflections were scaled using SCALEPACK (Otwinowski & Minor [1997] *Methods Enzymol* **276:**307-326). The structure factor amplitudes were calculated using TRUNCATE from the CCP4 program suite (French & Wilson [1978] *Acta Crystallogr **A*** **34:**517-525). The structure was solved by molecular replacement with the program PHASER (McCoy *et al* [2007] *J Appl Cryst* **40**:658-674), using as the starting model the refined structure of rhAChE complexed with fasciculin (Kryger *et al* [2000] *Acta Crystallogr **D*** **56:**1385-1394) (PDB code 1B41). All steps of atomic refinement utilized the CCP4/REFMAC5 program (Murshudov *et al* [1997] *Acta Crystallogr **D*** **53:**240-255). The model was built into $2mF_{obs} – DF_{calc}$ and $mF_{obs} - DF_{calc}$ maps using the COOT program (Emsley & Cowtan [2004] *Acta Crystallogr **D*** **60:**2126-2132). Refinement weights were optimized. The hAChE construct contains 543 amino acid residues. The final model includes residues Glu5-Ser541 (Fig. 5). The R_{free} value is 23.74% (based on the 5% of reflections not used in the refinement), and the R_{work} value is 19.31% for all data to 2.9 Å. The hAChE model was evaluated with the PROCHECK program (Laskowski *et al* [1993] *J Appl Cryst* **26:**283-291). The coordinates and structures factors have been deposited to the PDB and have been assigned PDB Code 4PQE.

The 4PQE crystal structure of rhAChE diffracts to 2.9 Å resolution, in the space group *$P3_112$*, with one monomer in the asymmetric unit. The structure of native rhAChE was earlier solved at 3.2 Å resolution in space group *$P6_1$* (PDB code 3LII) (Dvir *et al* [2010] *Chem Biol Interact* **187:**10-22), and at 2.16 Å resolution in space group *$P3_121$* (PDB code 4EY4) (Cheung *et al* [2012] *J Med Chem* **55:**10282-10286. In both cases the crystal structure revealed a dimer in the asymmetric unit. The structure of the hAChE monomer is characterized by an α/β-hydrolase fold that consists of a 12-stranded central mixed β-sheet surrounded by 14 α-helices. Three intramolecular disulfide bridges, Cys68-Cys95, Cys256-Cys271 and Cys408-Cys528, are seen. The functional hAChE dimer was generated using the two-fold crystallographic symmetry present in the *$P3_112$* space group. The subunits associate with each other by tight packing of two antiparallel α-helices from each subunit, α13 and α18-α19, which form a 4-helix bundle. The 4-helix bundle is a widely occurring structural motif for protein–protein interaction that takes place at the dimer interface between two monomers, each of which contributes two helices (Kohn *et al* [1997] *J Biol Chem* **272:**2583-2568; Lin *et al* [1995] *J Mol Biol* **248:**151-161). In many cases these helices are close to each other within the polypeptide sequence, being separated from each other by three loops (Kresse *et al* [2001] *Protein Eng* **14:**897-901). The interfaces between the helices consist mostly of hydrophobic residues, while polar side chains on the exposed surfaces interact with the aqueous environment. The macrodipoles of the two α-helices of the individual polypeptides are in a stabilizing anti-parallel arrangement (Fuxreiter & Simon [2002) *Proteins* **48:**320-326; Robinson & Sligar [1993] *Protein Sci* **2:**826-837). The 4-helix bundle is arranged in an up-and-down α13, α18-α19, α13', α18'-α19' topology, ↓↑↓↑. As a consequence, the active-site gorges of the two subunits face in opposite directions (Fig. 6). The 4-helix bundle is further stabilized by the interactions between conserved residues in the loop connecting α13 to α14 and residues from helices α18'-α19', and, conversely, between residues in the loop connecting α13' to α14' and residues from helices α18-α19. Non-polar residues point into the core of the bundle, while polar residues are oriented towards the aqueous solvent.

It is well established that the overall folds observed for the same protein crystallized in different space groups are usually very similar. However, local details of the structure may differ, especially the conformations of loops and surface side-chains. Side-chain conformations are determined by a combination of intramolecular and intermolecular forces. Thus, differences in surface side-chain conformations from space group to space group are due to different crystal packing constraints and/or variations in the ionic strength of the precipitant.

Comparison of the hAChE structure with other AChE and BChE structures

We performed a structure-based sequence comparison of the crystal structure of hAChE solved in the new space group *$P3_112$* with those of other AChEs (Table 1). hAChE crystal structures represent three different space groups, *$P3_112$ (*4PQE, *the present study), $P6_1$* (3LII; Dvir *et al* [2010] *Chem-Biol Interact* **187**:10-22) and *$P3_121$* (4EY4; Cheung *et al* [2012] *J Med Chem* **55**:10282-10286). Mouse AChE (mAChE) has been crystallized in the *$P2_12_12_1$* space group (PDB codes: 1MAA and 1J06, each with different cell dimensions) (Bourne *et al* [1999] *J Biol Chem* **274:**2963-2970; Bourne *et al*

[2003] *EMBO J* **22:**1-12); *Torpedo californica* AChE (*Tc*AChE) in three different space groups, $P2_12_12_1$, *C121* and $P3_121$, PDB codes: 1W75 Dvir *et al* [2002] *Biochemistry* **41:**10810-10818), 2J3D (Greenblatt *et al* [2004] *J Am Chem Soc* **126:**15405-15411), and 1EA5 (Harel *et al* [2006] unpublished data); *Drosophila melanogaster* AChE (*Dm*AChE) in space group $P4_32_12$, PDB code 1QO9 (Harel *et al* [2000] *Protein Sci* **9:**1063-1072; and *Electrophorus electricus* AChE (*Ee*AChE) in space groups *C121* and *F222.* Two *F222* crystal forms were described, with different unit cell parameters (PDB codes: 1C2B and 1EEA,Table 1), while the C121 crystal form was deposited as 1C2O,. All three *Ee*AChE structures were solved to limited resolution (>4 Å, Table 2), such that the *Ee*AChE residues could not be assigned unambiguously. Indeed, the coordinates deposited in the PDB are of the mAChE sequence for 1C2O and 1C2B (Bourne *et al* [1999] *J Biol Chem* **274:**30370-30376; Bourne *et al* [1999] *J Biol Chem* **274:** 2963-2970; Bourne *et al* [2003] *EMBO J* **22:**1-12), and of the *Tc*AChE sequence for 1EEA (Raves *et al* [1998] in *Structure and Function of Cholinesterases and Related Proteins*, Doctor, Taylor, Quinn, Rotundo & Gentry (eds), pp 351-356. New York: Plenum; Raves et al [1997] *Nat Struct Biol* **4:**57-63). The *Ee*AChE structures were, therefore, omitted from this comparative structural analysis.

Thus, we compared the orientations of 9 crystal structures of AChE from four different species in six different crystal forms. In some of these structures the asymmetric unit contains one or two homodimers, while in others it contains a single monomer, and the dimer is formed by a crystallographic 2-fold axis. The various structures contain 4-16 protein molecules in the crystallographic unit cell, such that there are 2-4 different monomer-monomer contacts in each unit cell of the various crystal forms. Our analysis revealed that all the crystal forms contain at least one physiological AChE dimer in the unit cell, with tight packing of two helices from each monomer producing the canonical cholinesterase 4-helix bundle. However, the crystal contacts between any other two adjacent subunits in the crystallographic unit cell significantly differ from one pair to the other, generating different non-physiological non-specific dimeric associations. For example, mAChE crystallized in $P2_12_12_1$ space group (PDB code 1J06), with 8 subunits in the unit cell (labeled A-H) with one physiological dimer AB, and three dimers - CD, EF and GH - related by crystallographic symmetry (Fig. 7) (Bourne *et al* [1999] *J Biol Chem* **274:**2963-2970). Several of the residues in the 4-helix bundle, including Glu376, Thr383, Asp384, Trp385, Gln508, Gln527, Phe535 and Lys538 (hAChE numbering), are strictly conserved in all three vertebrate species, but not in *Dm*AChE (Fig. 8). There are three distinct non-physiological dimers - AD, AG and AH - in mAChE (Bourne *et al* [1999] *J Biol Chem* **274:** 2963-2970) (Fig. 7). Analysis of the contacts between these non-physiological dimers revealed that they involve non-conserved residues, and that the residues are different in each of the three pairs, giving rise to different non-specific dimer associations. It should also be noted that they do not include any residues that are involved in forming the 4-helix bundle. These observations apply to all the space groups in the various species. Furthermore, the crystal contacts are much looser, *i.e.*, involve fewer interactions and fewer residues, in each of the non-specific dimers of the AChE structures, relative to the very tight association in the physiological dimers. Thus, for the hAChE and mAChE structures, the physiological dimer appears to be the one homologous to that in *Tc*AChE. Both the conservation of residues and the tighter

association thus support the notion that the dimers formed via the 4-helix bundle are, in fact, the physiological dimers (Table 1).

We evaluated the effect of crystal contacts on accessibility to the entrance of the active-site gorge. For each of the two subunits of the physiological dimer, we analyzed residues involved in close contacts, *i.e.*, up to 3.5 Å, with residues from neighboring subunits in the unit cell of the various crystal structures. In 5 of the 9 AChE crystal structures the crystal contacts with residues from symmetry-related subunits are located far from the entrance to the gorge. In four crystal forms, hAChE (PDB 4PQE), mAChE (PDB code 1MAA), *Tc*AChE (PDB code 1EA5) and hAChE (PDB code 3LII), these residues are near the entrance to the gorge of one of the two subunits forming the physiological AChE dimer. *Tc*AChE crystallized in P3121 space group (PDB code 1EA5) has 6 subunits in the unit cell (A-F), forming five subunit-subunit contacts (Fig. 9a). The two monomers that form the physiological dimer (AE), also form non-physiological dimers (AB, AC, ED and EF). The crystal-contacts between subunits A (part of the physiological AE dimer) and C, and between D and E (part of the physiological AE dimer) involve residues situated at the peripheral anionic site (PAS) that might, therefore, block accessibility to the active site (Fig. 9b). In the hAChE (PDB codes: 4PQE and 3LII) and mAChE (PDB code: 1MAA) structures some of the residues involved in crystal contacts are also close to the entrance of the gorge. As a result, accessibility to the entrance of the gorge of the neighboring subunit is partially restricted.

To further evaluate the effect of neighboring copies of the catalytic subunit in the various space groups we compared the electrostatic characteristics of the AChE dimers. The electrostatic potentials for the AChE monomer structures from various species have a negative external surface potential in the area around the entrance to the active-site gorge that becomes more negative as the rim of the gorge is approached Felder *et al* [1997] *J Molec Graphics & Modelling* **15**:318-327. The potential becomes increasingly more negative along the central axis running down the gorge, and is largest at the base of the gorge, near the active site. The active-site gorges of the two subunits in the physiological dimer face in opposite directions; consequently, the negative external surface potentials of each monomer point in opposite directions, i.e., the dipoles are related by the same 2-fold axis as the two monomers.

Since the AChE monomer displays an unusually large electrostatic dipole moment (Porschke *et al* [1996] *Biophys J* **70:**1603-1608), we were curious as to how it might affect the crystallographic packing and the accessibility of the entrance to the active-site gorge in the crystal. We calculated the electrostatic surface potentials of the individual AChE monomers in the different crystal forms. In *Tc*AChE the negative potential surface at the peripheral site of subunit E of the AE physiological dimer (black arrow in Fig. 9d) is adjacent to the positive potential surface of the symmetry-related subunit D (black arrow in Fig. 9c). Thus it is clear that the non-physiological dimer association between the ED subunits involves electrostatic complementarity.

The structures of the catalytic subunit monomers of the AChEs of the three vertebrate species, *h*AChE, mAChE and *Tc*AChE, show a very high degree of evolutionary conservation, displaying very limited conformational differences. *Dm*AChE displays somewhat larger deviations. The structural alignment of all the AChEs display root mean square deviations (RMSDs) that are consistent with the evolutionary distances and sequence differences between them (Fig. 8). Thus, hAChE shares ~88% sequence identity with mAChE, with an RMSD of 0.6-0.7 Å; 57% identity and an RMSD of 0.9 Å with *Tc*AChE, and an RMSD of 1.5 Å and 35.9% identity with *Dm*AChE (Table 1). The most pronounced differences between hAChE and *Dm*AChE are seen in the loop connecting α13 to α14 of the 4-helix bundle (residues Tyr382-Asp390 in hAChE and Tyr416-Gly424 in *Dm*AChE), with deviations ranging from 2.3 Å to 8.0 Å. In the vertebrate AChEs this loop points towards and close to its neighboring subunit, whereas in the *Dm*AChE structure it is positioned further away from the helix bundle axis, leading to misalignment in the dimer structure as compared to hAChE (Fig. 10).

Crystallization and structure analysis of the EMP-rhAChE conjugates

Attempts to obtain crystalline EMP-rhAChE conjugates were made by soaking 1 mM EMP-CHMC into crystals of native rhAChE as follows:

[+]-EMP-CHMC into rhAChE crystals grown from

- 14% PEG 20,000
- 0.1M imidazole, pH 8.0
- 0.5% ethyl acetate

[-]-EMP-CHMC and racemic EMP-CHMC into rhAChE crystals grown from

- 8% PEG 20,000
- 0.1M imidazole, pH 7.0
- 0.5% ethyl acetate

A total of four 24-well plates were set up for optimization of crystallization conditions. Crystals were grown at 4°C. Crystals of apo-rhAChE and those soaked with [+]-EMP-CHMC are shown in Fig. 11.

Data sets were collected at 100K, on beamline ID23-1, at the ESRF Grenoble, France, for rhAChE crystals into which [+]-EMP-CHMC had been soaked. Ten crystals were checked; most diffracted out to 3.3-3.7Å, with one diffracting to 2.7Å resolution (Fig. 12). A full data set for this latter crystal was collected. Six crystals of rhAChE soaked with [-]-EMP-CHMC, and two soaked with racemic EMP-CHMC, all failed to diffract well.

The data for the [+]-EMP-CHMC-soaked crystal were processed, and the 3D structure was determined by molecular replacement, using the WT rhAChE crystal structure (see above). Details of data collection and refinement statistics are shown in Table 3.

The initial difference electron density map clearly displayed density within the active site. Refinement revealed the OP moiety of EMP covalently attached to Ser-203 with the *S* configuration of the covalent adduct (Figs. 13 & 14). Fig. 15 shows that it forms H-

bonds with G121, G122 and A204, in the oxyanion hole, and with the catalytic histidine, H447. To the best of our knowledge, this is the first crystal structure of the human AChE with the less toxic R_P enantiomer of any nerve agent. Its importance is two-fold: firstly, the *S* configuration around the P atom in the covalent adduct is consistent with an in-line attack that results in reversal of the absolute configuration. Notably, in the case of the *O*-ethylmethylphosphonyl moiety, the priority rules of the ligands attached to the P atom maintain the same ranking before and after the displacement of the CHMC leaving group by the enzyme, and the formation of the covalent bond of the OP moiety with S203Oγ. Secondly, in view of the marked differences in the reaction rates for both spontaneous and oxime-induced reactivation, and in the velocity of the 'aging' reaction, for the hAChE conjugates of the S_P and R_P chiral forms of OP nerve agents (see, *e.g.*, de Jong & Klassen [1984] *Biochim Biophys Acta* **830**:345-348; Ordentlich *et al* [1999] *Biochemistry* **38**:3055-3066; Ordentlich *et al* [2004] *Biochemistry* **43**:11255-11265) the 3D structure of the adduct with the [+]-EMP-CHMC enantiomer that we present here provides a structural background for analyzing, head-to-head, the kinetic behavior of the two enantiomers of EMP-CHMC following phosphonylation of hAChE.

Effect of strain choice and expression conditions on hAChE expression in *E. coli*

hAChE and its Rosetta-designed homolog (Rosetta-hAChE) were synthetically synthesized after codon and GC-content optimization for expression in *E. coli*. They were cloned into a tag-less pET32 vector similarly to variant 3G4 (hAChE containing 21 back-to-ancestor mutations). The three variants were transformed into BL21(DE3) and Origami B cells and plated. Twenty-four single colonies were randomly picked for each variant, and used to inoculate 500 μl cultures grown at RT in Deep-96 Well plates. Overnight cultures were diluted 1:10 into fresh media and grown for 24h at RT, with or without IPTG induction (0.4 mM).

The cells were then pelleted (4,000 rpm, 4°C, 20 min) and lysed (200 μl lysis buffer, 37°C, 1200 rpm, 1 h), and the cell debris was spun down (4,000 rpm, 4°C, 20 min). The clear cell lysate supernatant was tested for AChE activity by the Ellman procedure.

All three variants express more soluble and active protein in Origami B cells than in BL21 (DE3) cells (Fig. 16). This can be attributed to the enhanced capacity for formation of disulfide bonds in the cytoplasm of the Origami B strain.

The Rosetta-variant of hAChE expresses 15-74-fold more active protein than wt hAChE, and 4-82-fold more active protein with respect to 3G4.

Unlike hAChE or 3G4, which are hardly expressed in BL21(DE3) cells, the Rosetta variant is expressed as active protein to a level only 2-fold lower than that obtained in Origami B. This suggests that the Rosetta-designed protein is folded into a stable conformation following expression, and that its disulfide bonds may be formed by air oxidation during the lysis of the cells. The folding of hAChE or 3G4 may be less efficient, which may preclude formation of the correct disulfide bonds upon oxidation.

IPTG induction increases the expression of folded protein by 4-24-fold in BL21(DE3) cells, whereas it decreases expression of folded protein by 1.3-10-fold in Origami B cells. Thus, “leaky” expression, in the absence of IPTG induction, seems to produce more folded and soluble protein in Origami B cells.

Effect of strain choice on hAChE expression in *E. coli* cells that enhance cytoplasmic disulfide bond formation

The presence of 3 intra-chain disulfide bonds in each hAChE monomer calls for expression of the protein in *E. coli* strains that enhance the formation of such bonds following translation and folding. Here we compared two strains that are used to express proteins that require disulfide bond formation to achieve their native conformation, namely, Origami B and SHuffle® T7 Express (NEB# C3029). Both come from an *E. coli* B strain background (Table 4).

Three variants of hAChE were expressed in Origami B or 3029H cells: **1.** hAChE in which codon and GC-content had been optimized for gene expression in *E. coli*; ***2.*** Rosetta-hAChE, an hAChE variant with 43 designed mutations that was codon and GC-content optimized for expression in *E. coli*; **3.** 3G4, a variant of hAChE containing 21 ancestral mutations). The cultures (2.5 ml 2YT supplemented with Amp 100 μg/ml) were grown from single colonies at 37°C, with shaking at 250 rpm. After 2h growth to an OD_{600nm} of 0.3-0.4, gene expression was induced by IPTG (0.4 mM), and growth was continued at 20°C for ~16 h.

Cells were pelleted by centrifugation (14,000 rpm, 10 min), and resuspended in lysis buffer (20 mM Tris-HCl, pH 8.0, 100 mM NaCl, 10% glycerol, 0.1% Triton X-100, Benzonase nuclease 1:5,0000, 0.2 mg/ml lysozyme) to OD_{600nm} = 8. They were lysed at 37°C for 1.5 h with shaking (1,200 rpm). The cell debris was pelleted (14,000 rpm, 4°C, 15 min). Aliquots of 5μl of clear cell lysate from each culture tube were pipetted into a 96-well ELISA plate.

AChE activity of the lysates was measured by addition of 0.55 mM acetylthiocholine and 0.85 mM DTNB to each well, to a final volume of 200μl, followed by monitoring at 412 nm for 5 min.

Before induction (Fig. 17), cultures of both *E. coli* strains grew to a similar cell density, while after induction, followed by growth overnight at 20°C, the 3029H cultures contained 2.5-3.5 fold more cells than the Origami B cultures expressing the same proteins (Fig. 18). There was no significant difference in the toxicity of the three variants in either growth strain (*i.e.,* cell density was not affected by the identity of the variant). The activity of all three variants was similar in the two strains (Fig. 19).

Thus, while the final concentration of AChE protein per cell seems to be roughly the same for both the Origami B and 3029H strains, the latter produces a much larger number of cells after induction. Thus, the 3029H strain will be selected for large-scale growth since it is likely to produce substantially higher yields of purified protein.

3. KEY RESARCH ACCOMPLISHMENTS

- Cloning and expression of the WT rhAChE monomer in HEK293 cells
- Purification and characterization of rhAChE
- Deglycosylation of the expressed rhAChE
- Crystallization of the expressed rhAChE
- X-ray data collection of rhAChE
- 3D structure determination of rhAChE
- Cloning and expression of rhAChE$_T$ in HEK293 cells
- Affinity purification of rhAChE$_T$
- Characterization of rhAChE$_T$
- Deglycosylation of rhAChE$_T$
- Tetramerization of DG-rhAChE$_T$
- Synthesis of the pure chiral forms of the coumarin surrogate VX, both the toxic S_p isomer, and the much less reactive and less toxic R_p form, in accordance with our published protocol, permitted preparation of the corresponding crystalline OP/hAChE conjugates. The crystal structure of the R_p conjugate has been solved to 2.7 Å.
- Computational design, together with strain selection, have permitted major progress in the expression of soluble and catalytically active variants of hAChE in *E. coli*.

4. REPORTABLE OUTCOMES

Presentations:

- 14th ISCM in Hangzhou, China (May 2013) by Joel L. Sussman, title: "Acetylcholinesterase: From 3D Structure to Dynamics
- ICSG2013-SLS, Sapporo, Japan (Jul 2013) by Joel L. Sussman, title: "Cholinesterases: From 3D Structure to Dynamics"
- Invited Lecture at Regional Centre for Biotechnology, Gurgaon, India (Sep, 2013) by Joel L. Sussman, title: "Molecular Basis of How Nerve Agents through anti-Alzheimer Drugs Function: 3D Structure of Acetylcholinesterase"
- Regional Centre for Biotechnology, Gurgaon, India (Sep 2013) - Keynote Lecture by Joel L. Sussman, title: "Molecular Basis of How Nerve Agents through anti-Alzheimer Drugs Function: 3D Structure of Acetylcholinesterase
- Florida International University (FIU), Miami, FL (Dec 2013) - Invited Lecture by Joel L. Sussman, title: "Molecular Basis of anti-Alzheimer Drugs & Nerve Agents: 3D Structure of Acetylcholinesterase"
- Technion, Haifa, ISRAEL (Dec 2013) - Invited Lecture by Joel L. Sussman, title: "Molecular Basis of How Nerve Agents & anti-Alzheimer Drugs Function: 3D Structure of Acetylcholinesterase"
- 19th Biennial Medical Defense Bioscience Review, Hunt Valley, MD (May 2014) - Invited Clarence A. Broomfield Award Lecture by Joel L. Sussman, title: "Acetylcholinesterase – From 3D Structure to Function: Impact on Drug Discovery and Protection Against Chemical Threat Agents"
- Invited Lecture, University of Oulu, Oulu, (March, 2015) "What is in Common between Alzheimer's Drugs & Nerve Agents? Acetylcholinesterase"

5. CONCLUSIONS

The human acetylcholinesterase (hAChE) gene was cloned into the pHLsec expression vector. It was expressed on a large-scale, utilizing 64 large plates (15 cm) of adherent 293T cells. The recombinant human AChE (rhAChE) was purified by affinity chromatography, and deglycosylated with PNGase F, thus producing a highly purified preparation from which it was possible to obtain rhAChE crystals that diffracted to 2.9 Å. This, in turn, permitted 3D structure determination and refinement. The data were deposited in the PDB (IDcode 4PQE).

The major outcome of the structural information provided by this research is the potential to develop one or more products based on a combination of hAChE with one or more oxime reactivators that will act synergistically to perform pseudocatalytic hydrolysis of all V- or G-agents. It is envisaged that these products will be utilized either prophylactically or in a post-treatment context. Embedded in a suitable medical doctrine they will expedite the recovery and return to full battle capability of the war-fighter. The approach adopted should substantially reduce the amount of enzyme protein required to afford protection, thus making its availability more economically feasible. The civilian population may be exposed to OP nerve agents both in military and terrorist scenarios. However, civilians are also exposed to and susceptible to a variety of commercially available OP-based and carbamate-based insecticides in both a domestic and an agricultural context. The same considerations outlined above may thus also be pertinent to treatment of civilians. The issue of reduced protein dosage, resulting in enhanced cost effectiveness, will be particularly relevant to the civilian arena, where treatment may be administered to a large and heterogeneous population in terms of age and medical background.

The synergistic and parallel approach of expression of hAChE in the human HEK293 cell line, together with the use of a computational approach to achieve expression of soluble and active hAChE in *E. coli*, position us to perform structure/function studies of the interaction of OP nerve agents and reactivators of the OP-AChE conjugates with both wt hAChE and with suitably designed variants.

Future Plans

- To increase the yield of the recombinant hAChE by testing expression in transiently transfected 293E cells, and to grow large quantities in suspension cultures.
- To purify and characterize the rhAChEG4 construct.
- To initiate experiments on soaking OP surrogates into native crystals of rhAChEmD already obtained, and subsequently into rhAChEG4 crystals, which likely will correspond to the physiological tetramer.
- To determine the kinetics of interaction of the nerve agent surrogates with the expressed constructs, as well as the rates of aging of the inactive OP conjugates thus obtained, and of their reactivation by suitable oximes.
- Initiation of crystallization screens of G-agent/rhAChE conjugates obtained by interaction of the enzyme with G-agent surrogates.

- rhAChE will continue to be expressed in a eukaryotic system, *viz.*, in HEK293 cells. Use of the eukaryotic system permits expression of the enzyme as functional oligomers that resemble those occurring *in situ*, and also bear similar post-translational modifications.
- We will soak additional chiral OP nerve agent surrogates, or the agents themselves generated *in situ*, into crystals of wt rhAChE, produced in 293 cells (as reported previously), and of suitable rhAChE variants expressed in *E. coli*. Alternatively, we will react the enzyme and the OPs in solution, and crystallize the conjugates thus obtained.
- Crystals of the conjugates of rhAChEs with the OP nerve agents will be used for structure determination, followed by analysis of the 3D structures.

6. APPENDICES

None.

7. SUPPORTING DATA

Tables:

Table 1: Crystal structures and crystal contacts for 3D AChE structures

Species	Space Group	Crystal Form	PDB	Seq ID (%)	# dimer contacts	Number of crystallographic contacts	AU	UC
human	$P3_111$	trigonal	4PQE	100	26	14	1	6
human	$P6_1$	hexagonal	3LII	100	26	11	2	12
human	$P3_121$	trigonal	4EY4	100	31	3-16	2	12
mouse	$P2_12_12_1$	orthorhombic	1J06	88.6	30	6-20	2	8
mouse	$P2_12_12_1$	orthorhombic	1MAA	88.6	26	10-22	4	16
Torpedo	$P2_12_12_1$	orthorhombic	1W75	57.5	11	2-8	2	8
Torpedo	C121	monoclinic	2J3D	57.5	23	19	1	4
Torpedo	$P3_121$	trigonal	1EA5	57.5	21	19	1	6
Electrophorus[1]	C121	monoclinic	1C2O	88.5	--	--	4	16
Electrophorus[1]	F222	orthorhombic	1C2B	88.5	--	--	1	16
Electrophorus[2]	F222	orthorhombic	1EEA	88.5	--	--	-	--
Drosophila	$P4_32_12$	tetragonal	1QO9	35.9	25	2-15	1	8

[1] In the 1C2O and 1C2 PDB structures the sequence of mAChE was used due to the low resolution of the X-ray data; thus it does not seem useful to generate a list of crystallographic contacts, etc.

[2] In the 1EEA PDB structure the sequence of *Tc*AChE was used due to the low resolution of the X-ray data; thus it does not seem useful to generate a list of crystallographic contacts, etc.

Table 2: Crystallization and crystallographic data for crystal forms of AChEs

Species (PDB ID Code)	Space Group	Cell Dimensions	RMSD to new Å	Res Å	Seq identity to human (%)	Crystallization conditions
Human (4PQE)	$P3_111$	a=b= 125.31 c=131.39 γ=120		2.90	100	0.1 M imidazole, pH=7 12% PEG 20,000 0.5% ethyl acetate
Human (3LII)	$P6_1$	a=b= 210.90 c=115.27 γ=120	0.525	3.20	100	1.3–1.5 M $(Li)_2SO_4$ 0.1 M HEPES, pH=6.8
Human (4EY4)	$P3_121$	a=b= 106.18 c=324.39 γ=120	0.502	2.16	100	15-21% PEG 3,350 0.17-0.21 M KNO_3
Mouse (1J06)	$P2_12_12_1$	a=79.19 b=111.97 c=226.83 α=β=Y=90	0.635	2.35	88.6	25-32% PEG 600 25-100 mM HEPES or sodium acetate, pH 6.5–8.0
Mouse (1MAA)	$P2_12_12_1$	a=136.55 b=173.13 c=224.25 α=β=Y=90	0.632	2.90	88.6	1.7 M $NaKPO_4$, pH=7.0 10 mM $CaCl_2$
Torpedo (1W75)	$P2_12_12_1$	a=91.50 b=106.58 c=150.34 α=β=Y=90	0.632	2.40	57.5	40% PEG200 0.5M MES pH=5.8
Torpedo (2J3D)	C121	a=128.74 b=105.49 c=70.60 β= 106.62	0.947	2.60	57.5	30% PEG 400 0.1M Tris pH=8.5 0.2M $MgCl_2$ PEG 550MME
Torpedo (1EA5)	$P3_121$	a=b= 111.57 c=137.59 γ=120	0.947	1.80	57.5	38% PEG 200 0.1 M MES, pH=8.0
Electrophorus (1C2O)	C121	a=211.16 b=129.75 c=195.42 β= 103.20	0.691	4.20	88.5	1.1–1.5 M $NaKPO_4$ pH 8.0–9.5
Electrophorus (1C2B)	F222	a=117.98 b=215.87 c=229.41 α=β=Y=90	0.691	4.50	88.5	1.4 M $(NH_4)_2SO_4$, pH 5.5–6.0
Electrophorus (1EEA)	F222	a=140.86 b=201.46 c=237.77 α=β=Y=90	0.738	4.50	88.5	500 mM NaCl
Drosophila (1QO9)	$P4_32_12$	a=b= 94.34 c=159.00 α=β=Y=90	1.463	2.70	35.9	13% PEG MME 2,000 0.1 M $(NH_4)_2SO_4$ 0.03 M leucine 0.1 M sodium acetate, pH=4.6

Table 3. Data collection and crystallographic refinement statistics of hAChE and [+]-EMP-hAChE

	hAChE	**[+]-EMP hAChE**
Data collection		
Collected at	ID23-2	ID23-1
Resolution range (Å)	50.0–2.9 (2.95–2.9)[a]	44.8–2.75 (2.9–2.75)[a]
Space group	*$P3_112$*	*$P3_112$*
Unit cell dimensions (*a, b, c* (Å))	125.3, 125.3, 131.4	124.4, 124.4, 129.1
β (°)	120	120
Number of molecules in the asymmetric unit	1	1
Number of reflections measured	286,078	123,580
Number of unique reflections	26,326 (1,287)[a]	29,752 (4,328)[a]
R_{sym}	0.127 (0.52)[a]	0.100 (0.54)[a]
Completeness (%)	99.9 (100.0)[a]	99.6 (99.4)[a]
Redundancy	10.9 (10.9)[a]	4.2 (3.9)[a]
<I>/<s(I) >	17.8 (4.4)[a]	13.1 (2.8)[a]
Refinement statistics		
Resolution (Å)	50-2.9	41.9–2.9
Rwork (%)	19.0	21.3
Rfree (%)	23.6	26.7

[a]Values in parentheses correspond to the highest-resolution shell

Table 4. Genotype and properties of *E. coli* strains used for expression.

Strain	**Bacterial strain origin**	**Genotype**	**Properties**
Origami B (DE3) Novagen®	*E. coli* B	F- *ompT hsd*S_B(r_B- m_B-) *gal dcm lacY1 ahpC* (DE3) *gor522*:: Tn*10 trxB* (Kan^R, Tet^R)	Origami B host strains carry the same trxB/gor mutations as the original Origami strains, except that they are derived from a lacZY mutant of BL21. Thus the Origami B strains combine the desirable characteristics of BL21, Tuner&trade and Origami in one strain background.
SHuffle® T7-Express C3029H NEB®	*E. coli* B	*fhuA2 lacZ::T7 gene1 [lon] ompT ahpC gal λatt::pNEB3-r1-cDsbC (*$Spec^R$*, lacI*^{q}*) ΔtrxB sulA11 R(mcr-73::miniTn10--*Tet^S*)2 [dcm] R(zgb-210::Tn10 --*Tet^S*) endA1 Δgor Δ(mcrC-mrr)114::IS10*	SHuffle has deletions of the genes for glutaredoxin reductase and thioredoxin reductase (Δgor ΔtrxB), which allows disulfide bonds to form in the cytoplasm. This combination of mutations is normally lethal, but the lethality is suppressed by a mutation in the peroxiredoxin enzyme (ahpC*). In addition, SHuffle expresses a version of the periplasmic disulfide bond isomerase DsbC that lacks its signal sequence, retaining it in the cytoplasm. This enzyme has been shown to act on proteins with multiple disulfide bonds, to correct mis-oxidized bonds and promote proper folding. The gene for the cytoplasmic DsbC is present on the chromosome.

Figures:

```
EGREDAELLVTVRGGRLRGIRLKTPGGPVSAFLGIPFAEPPMGPRRFLPPEPKQPWSGVVDATT
FQSVCYQYVDTLYPGFEGTEMWNPNRELSEDCLYLNVWTPYPRPTSPTPVLVWIYGGGFYSGAS
SLDVYDGRFLVQAERTVLVSMNYRVGAFGFLALPGSREAPGNVGLLDQRLALQWVQENVAAFGG
DPTSVTLFGESAGAASVGMHLLSPPSRGLFHRAVLQSGAPNGPWATVGMGEARRRATQLAHLVG
CPPGGTGGNDTELVACLRTRPAQVLVNHEWHVLPQESVFRFSFVPVVDGDFLSDTPEALINAGD
FHGLQVLVGVVKDEGSYFLVYGAPGFSKDNESLISRAEFLAGVRVGVPQVSDLAAEAVVLHYTD
WLHPEDPARLREALSDVVGDHNVVCPVAQLAGRLAAQGARVYAYVFEHRASTLSWPLWMGVPHG
YEIEFIFGIPLDPSRNYTAEEKIFAQRLMRYWANFARTGDPNEPRDPKAPQWPPYTAGAQQYVS
LDLRPLEVRRGLRAQACAFWNRFLPKLLSAT
```

Fig. 1. Amino acid sequence of the hAChEmD construct, which corresponds to the entire mature huAChE sequence, 32-574 (UniProt - P22303; Soreq *et al* [1990] *PNAS* **87**: 9688-92).

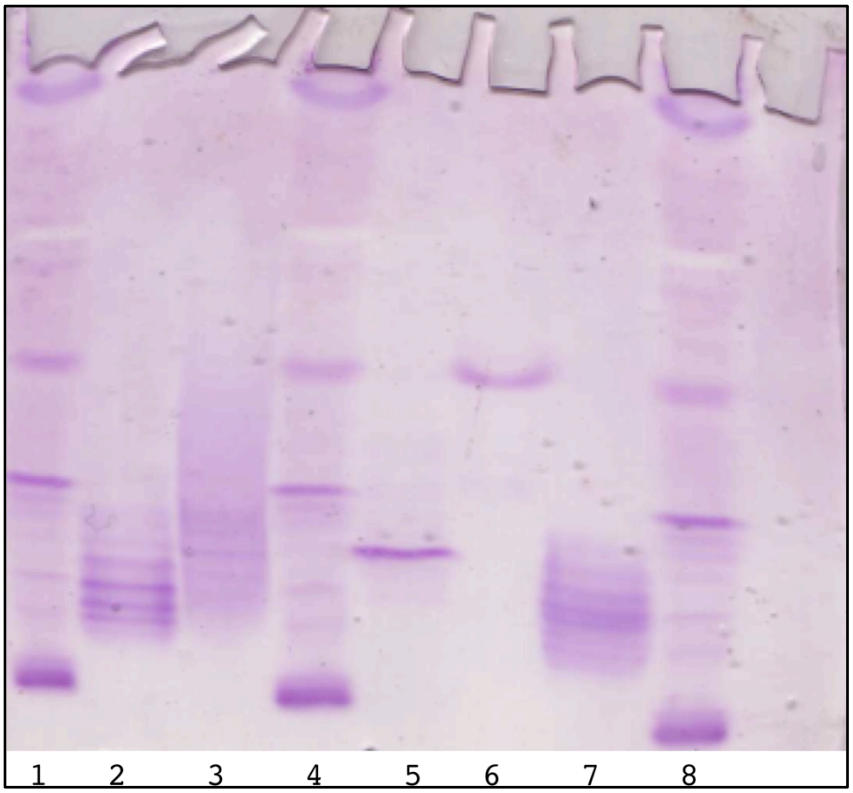

Fig. 2: Isoelectric focusing (IEF) of rhAChE before and after deglycosylation performed on a Bio Rad Ready Gel Plate PI5-8. Staining was with Coomassie Blue R250 together with Scarlet Red. Lanes 1, 4, 8: IEF markers; Lane 2: rhAChE before deglycosylation; Lane 3: *Torpedo californica* AChE; Lane 5: bovine erythrocyte carbonic anhydrase isozyme II (PI = 5.4); Lane 6: human erythrocyte carbonic anhydrase isozyme I (PI = 6.5); Lane 7: rhAChE after deglycosylation.

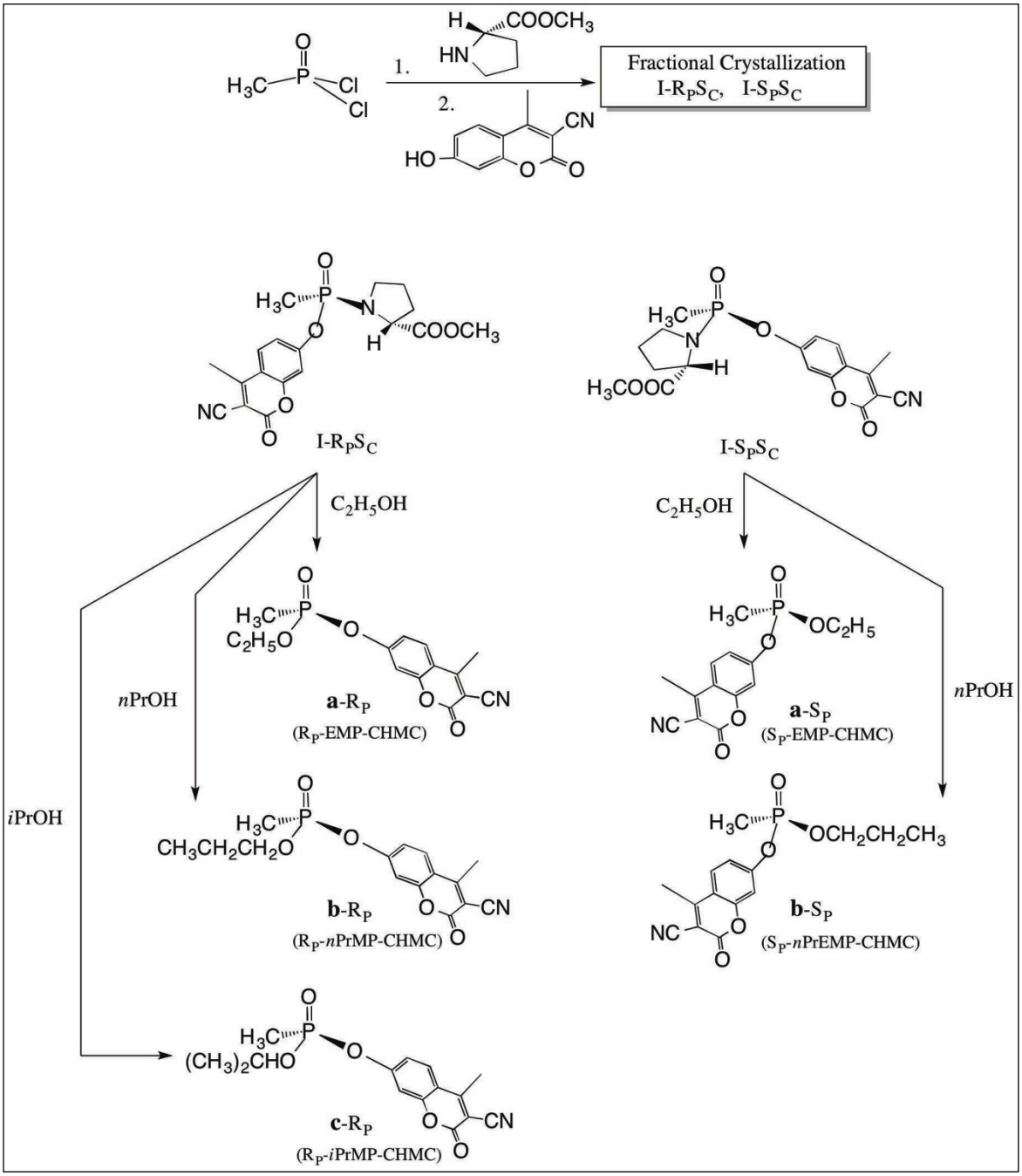

Fig. 3. **Stereospecific synthesis of R_P- and S_P-*O*-alkyl methylphosphonyl-CHMC esters from methylphosphonyl dichloride [$CH_3P(O)Cl_2$], l-proline methyl ester, and 3-cyano-7-hydroxy-4-methylcoumarin (CHMC).** The indicated absolute configuration was determined by X-ray diffraction of the corresponding crystals and by enzymatic hydrolysis. Alcoholysis was catalyzed by 1M H_2SO_4. The synthetic pathway for obtaining the chiral forms of CMP-CHMC is shown.

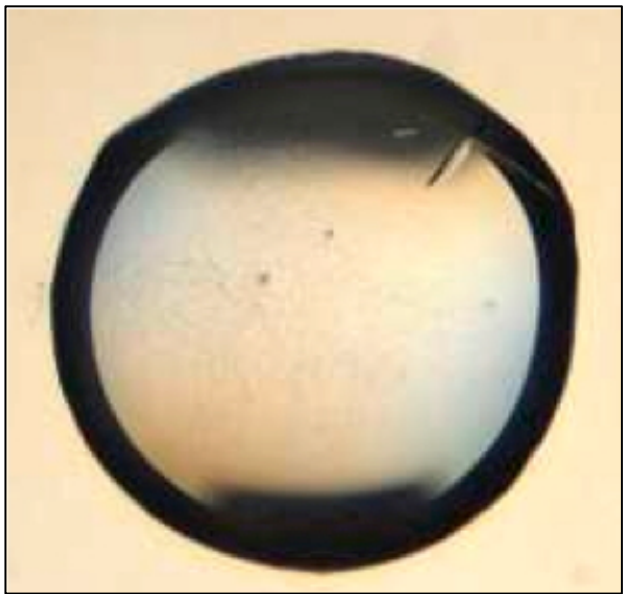

Fig. 4. Crystals of rhAChEmD, grown in sitting drops from a solution of 100 mM imidazole pH=7.0/12% polyethylene glycol 20,000. These crystals diffracted to 2.9Å resolution.

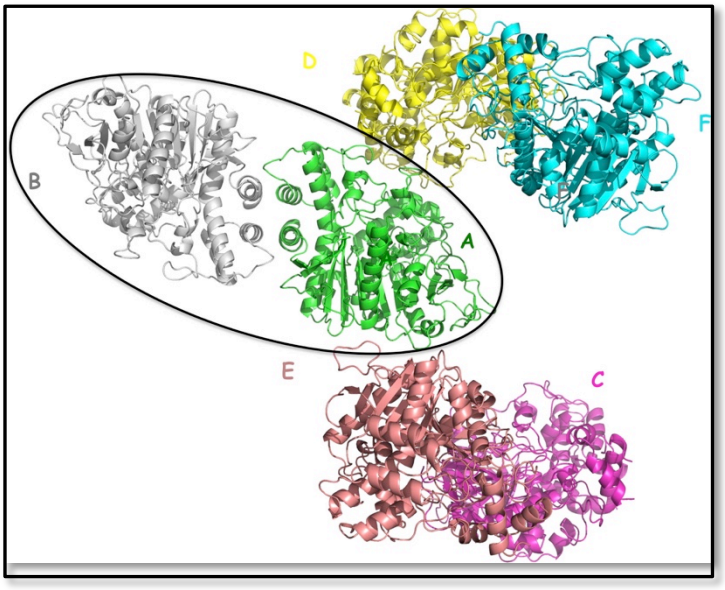

Fig. 5. Crystal packing of rhAChEmD solved to 2.9 Å in space group $P3_112$

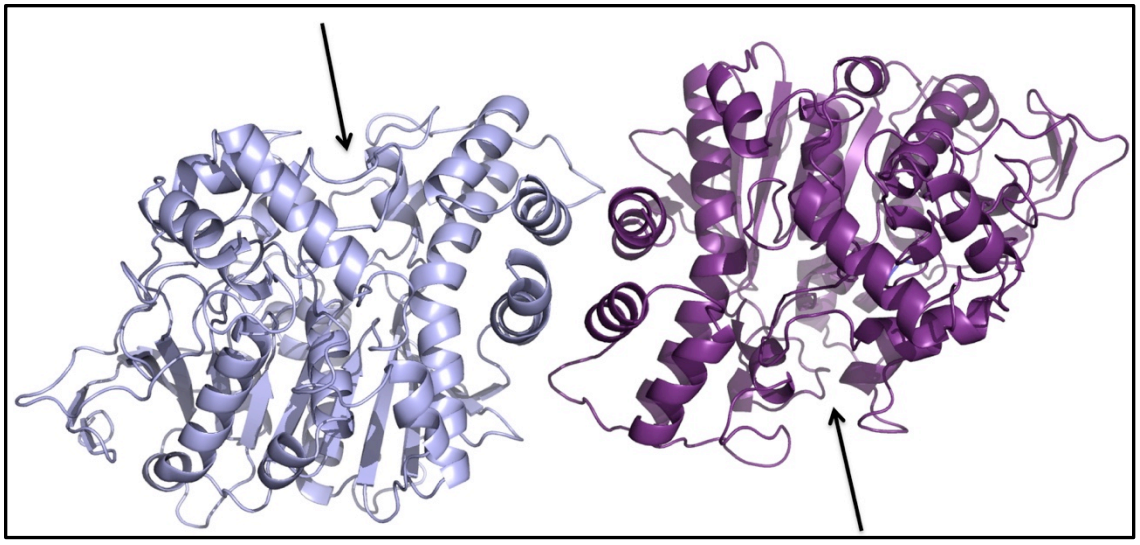

Fig. 6. Molecular dimer as seen in the rhAChE crystal structure. View is down the crystallographic 2-fold axis, showing the 4-helix bundle, with black arrows indicating the entrances to the active-site gorges of the two subunits that face in opposite directions

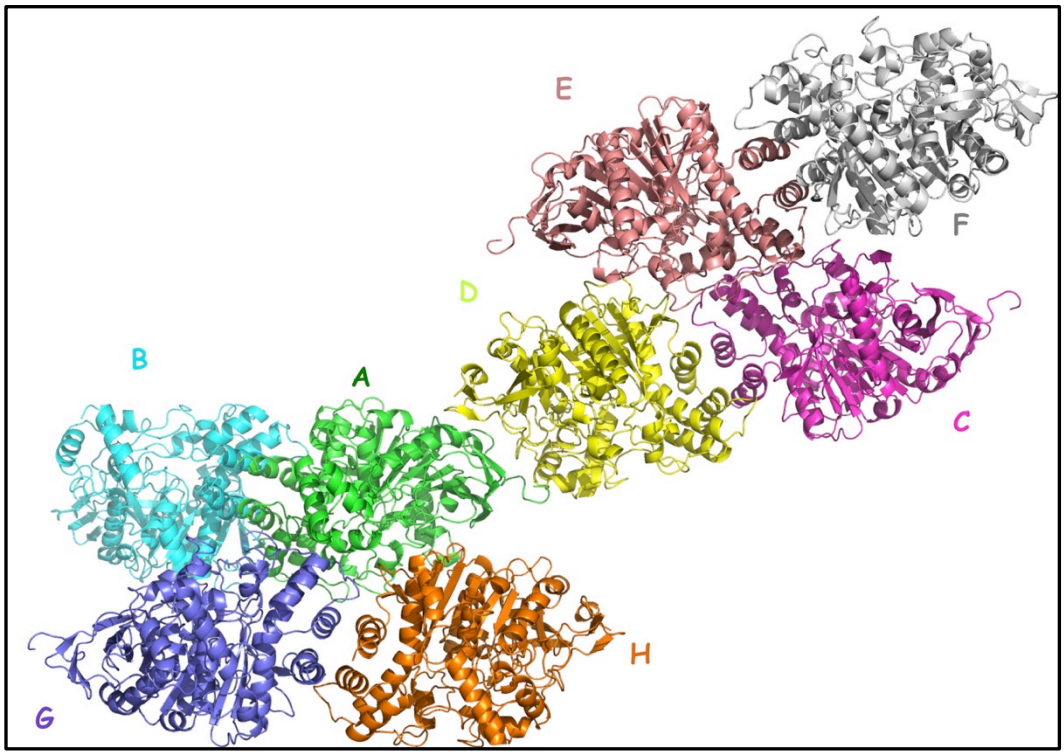

Fig. 7. Symmetry-related molecules in the $P2_12_12_1$ space group of mAChE (PDB1JO6)

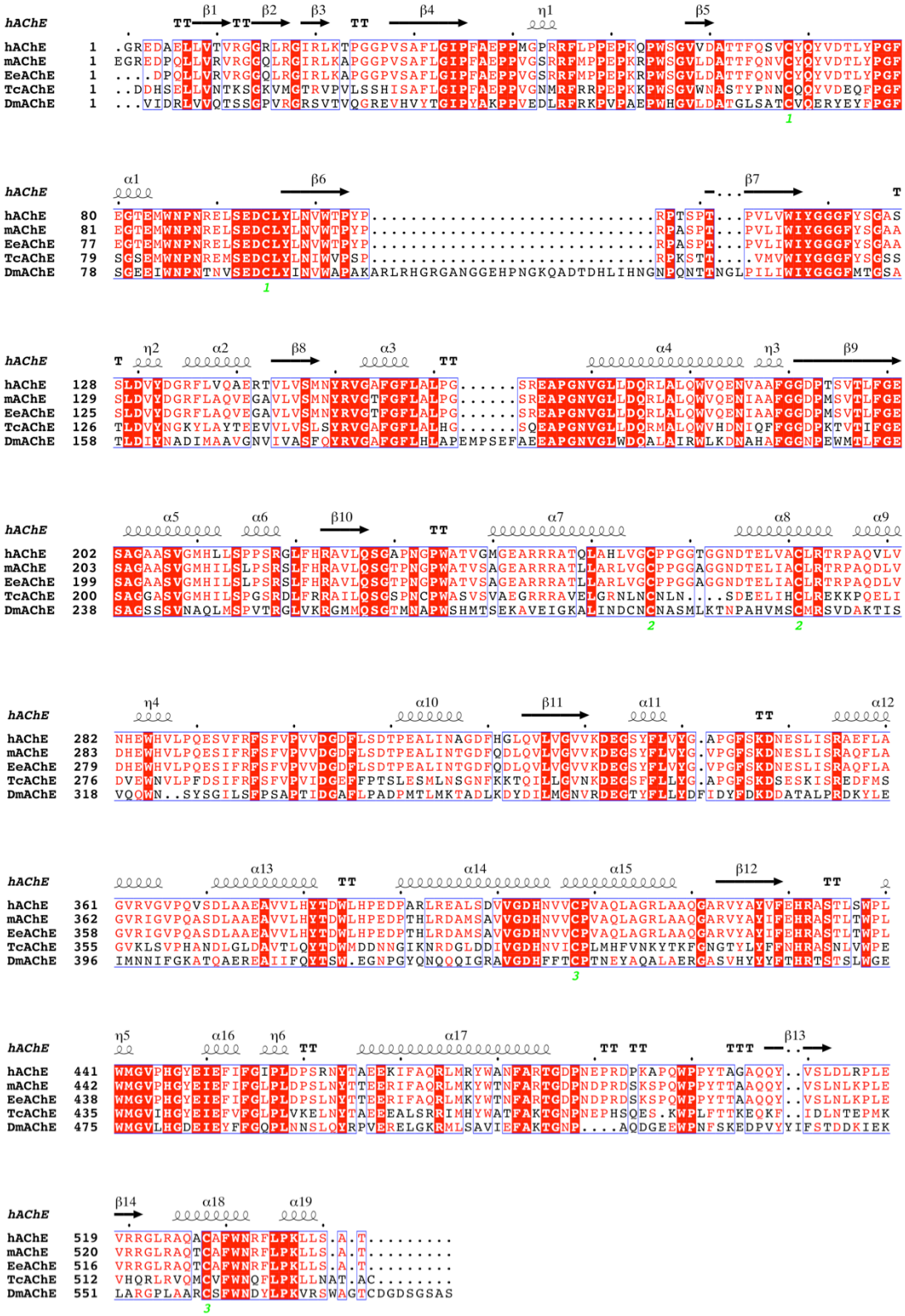

Fig. 8. Sequence alignment of AChEs whose 3D structures have been solved

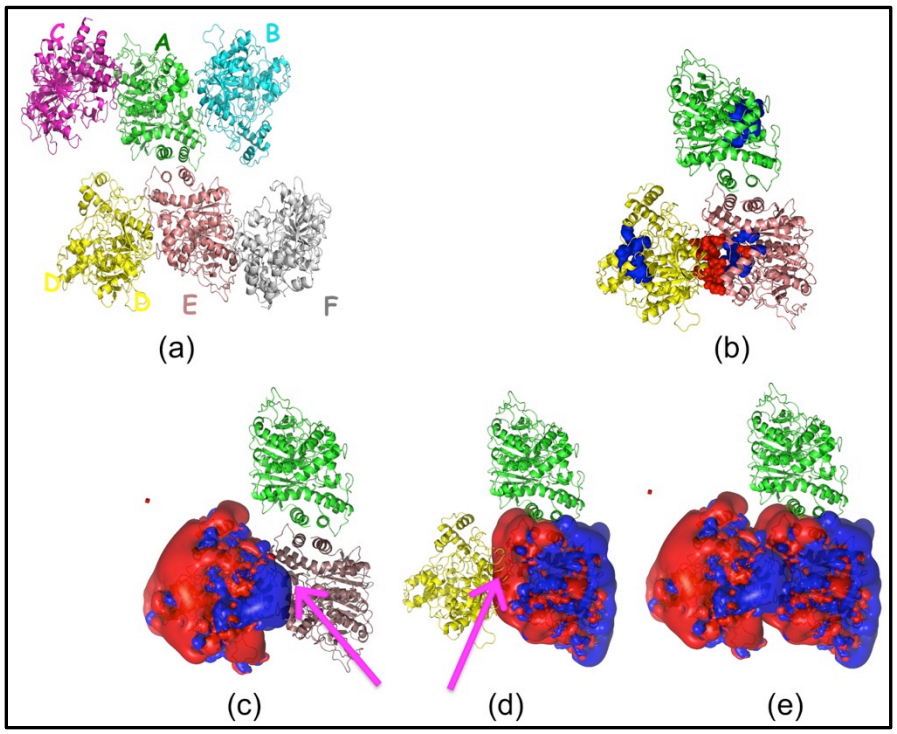

Fig. 9. Crystallographic packing and electrostatic interactions of *Tc*AChE (PDB Code 1EA5). (a) Crystallographic packing in space group $P3_121$; (b) representation in which the active-site residues are shown as blue balls, and the crystal contacts at the entrance to the gorge are shown in red; (c) monomer D (colored yellow in (b)), with its electrostatic surface colored red for negative potential and blue for positive potential, which forms a non-physiological contact with monomer E, with a pink arrow pointing towards the peripheral anionic site on monomer E; (d) monomer E (colored violet in (b)), with its electrostatic surface colored red for negative potential and blue for positive potential, which forms a non-physiological contact with monomer D, with a pink arrow pointing towards the peripheral anionic site on monomer E; (e) monomers D and E with their electrostatic surfaces colored red for negative potential and blue for positive potential.

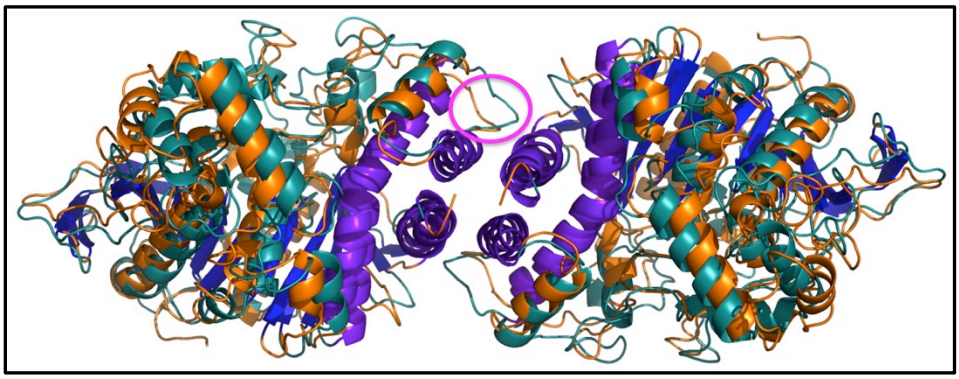

Fig. 10. Alignment of rhAChE (cyan) and *Dm*AChE (orange), displaying the tight alignment of the β sheets (blue) and of the 4-helix bundle (purple), but larger divergence of the rest of the helices. The region with the most pronounces differences between hAChE and *Dm*AChE is in the loop connecting α13 to α14 of the 4-helix bundle (residues Tyr382-Asp390 in hAChE and Tyr416-Gly424 in *Dm*AChE), and is circled in magenta.

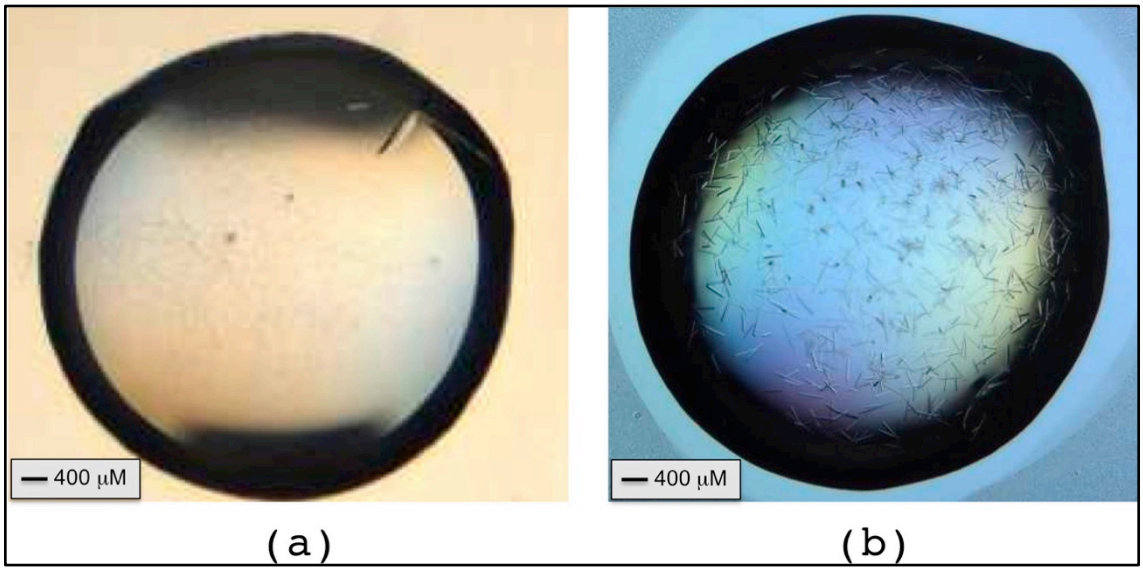

Fig. 11. Crystals of (a) apo-rhAChE; (b) rhAChE complexed with [+]-EMP.

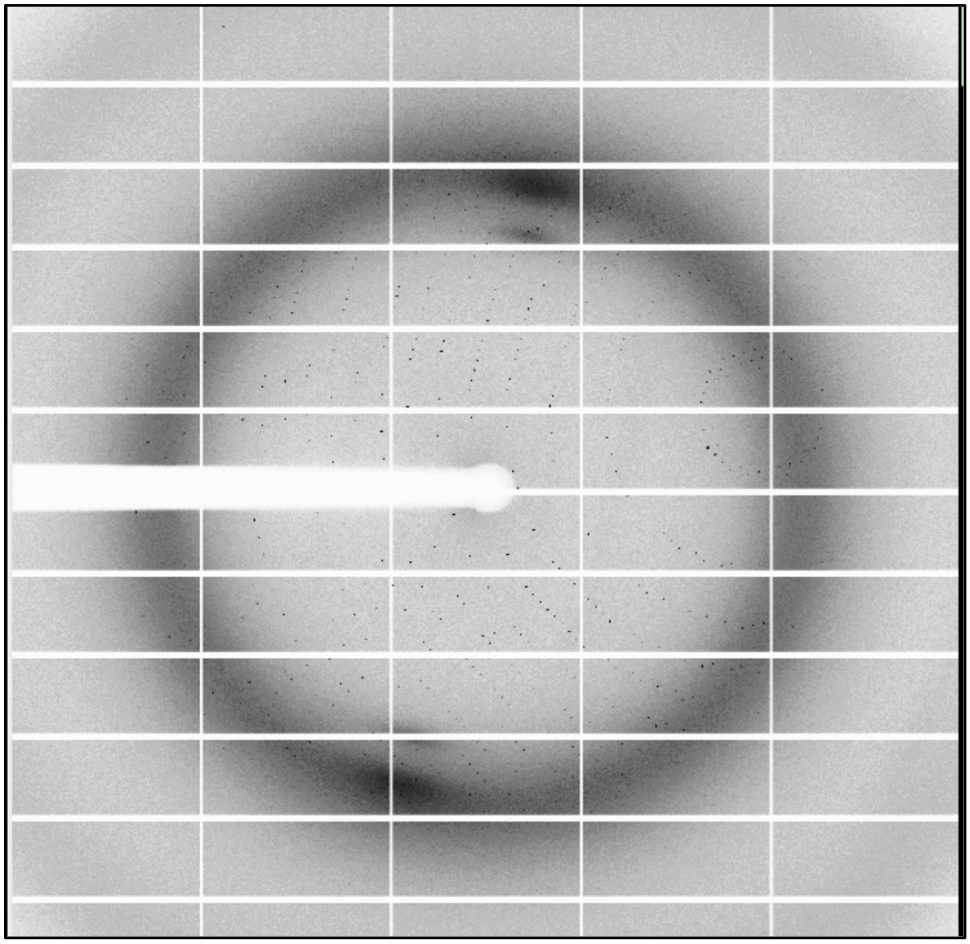

Fig. 12. Representative image of the X-ray diffraction pattern to 2.75Å resolution, collected for the +EMP/hAChE conjugate on beamline ID23-1 at the ESRF.

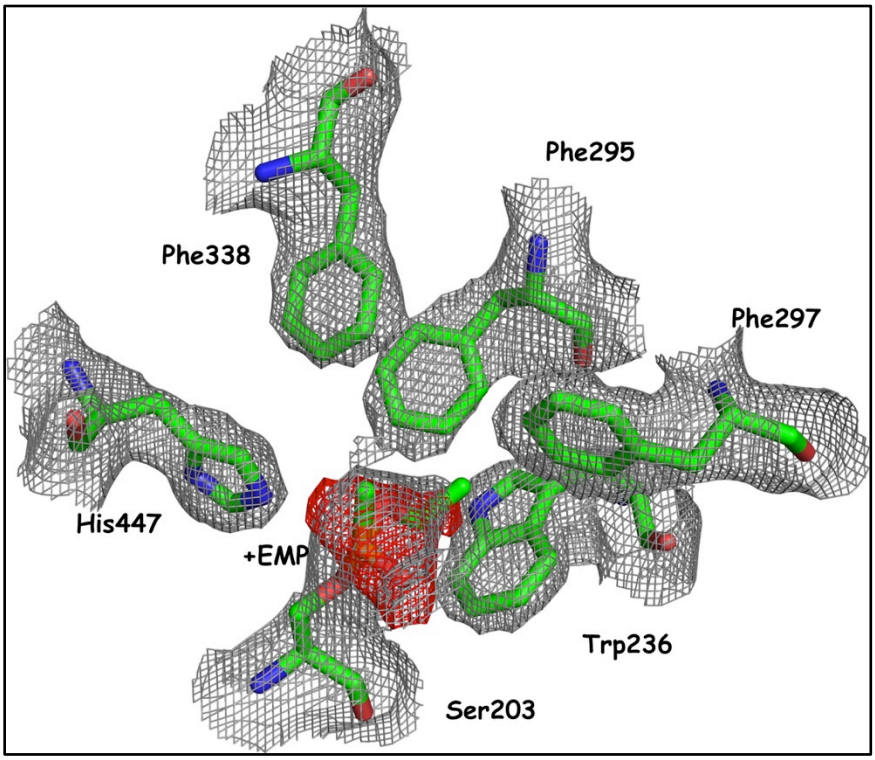

Fig. 13. Electron density of the active site of the [+]-EMP/hAChE conjugate.

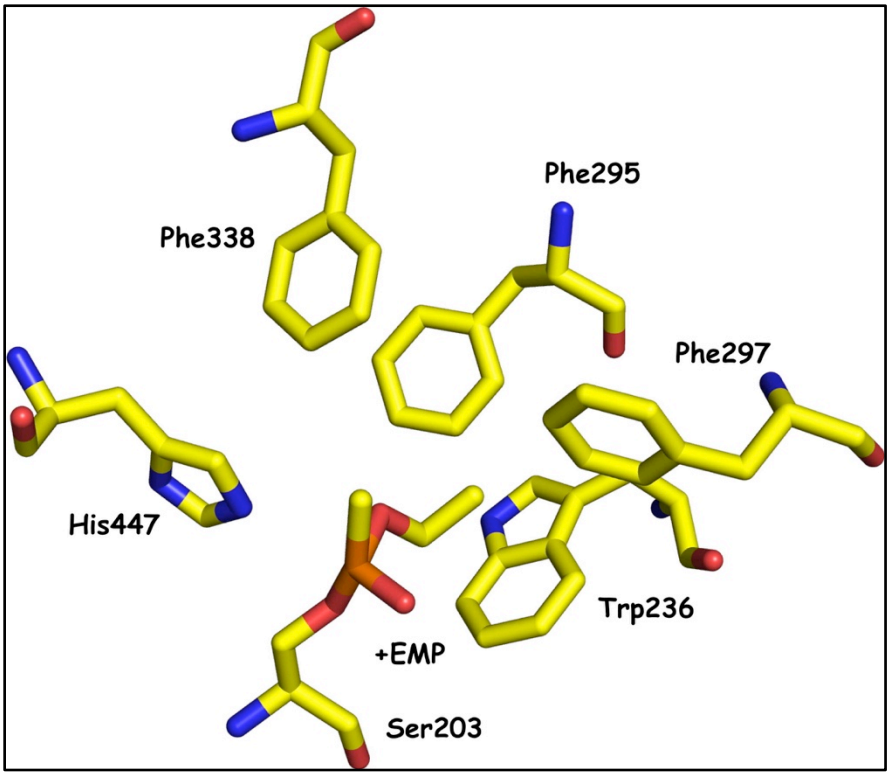

Fig. 14. Three-dimensional fit of [+]-EMP, and of amino acid residues within the active site, into the electron density (shown in the same orientation as in Fig. 13).

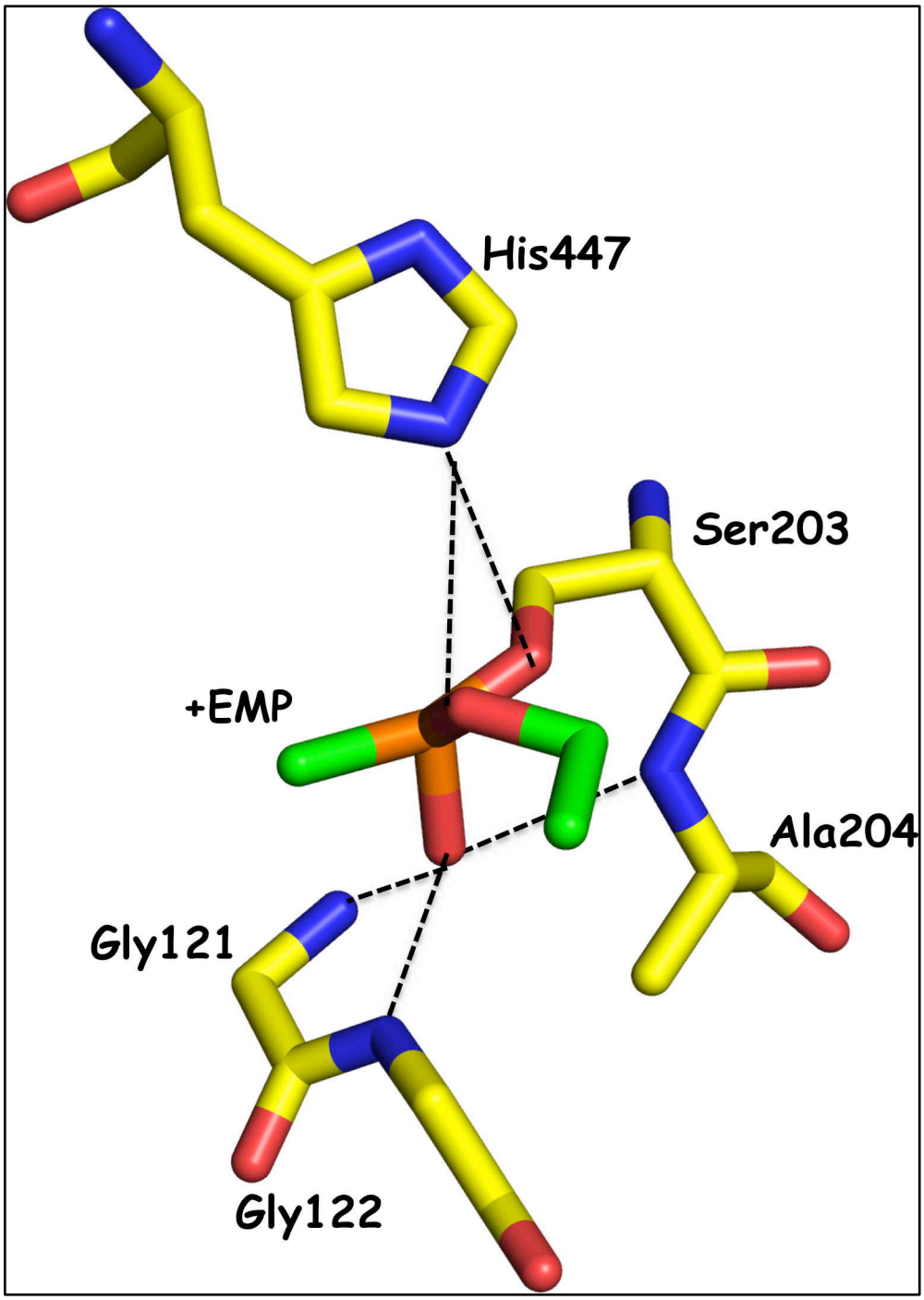

Fig. 15. Stick figure displaying the active-site region of the [+]-EMP/hAChE conjugate, highlighting H-bonds to G121, G122 and A204, within the oxyanion hole, and to the catalytic H447.

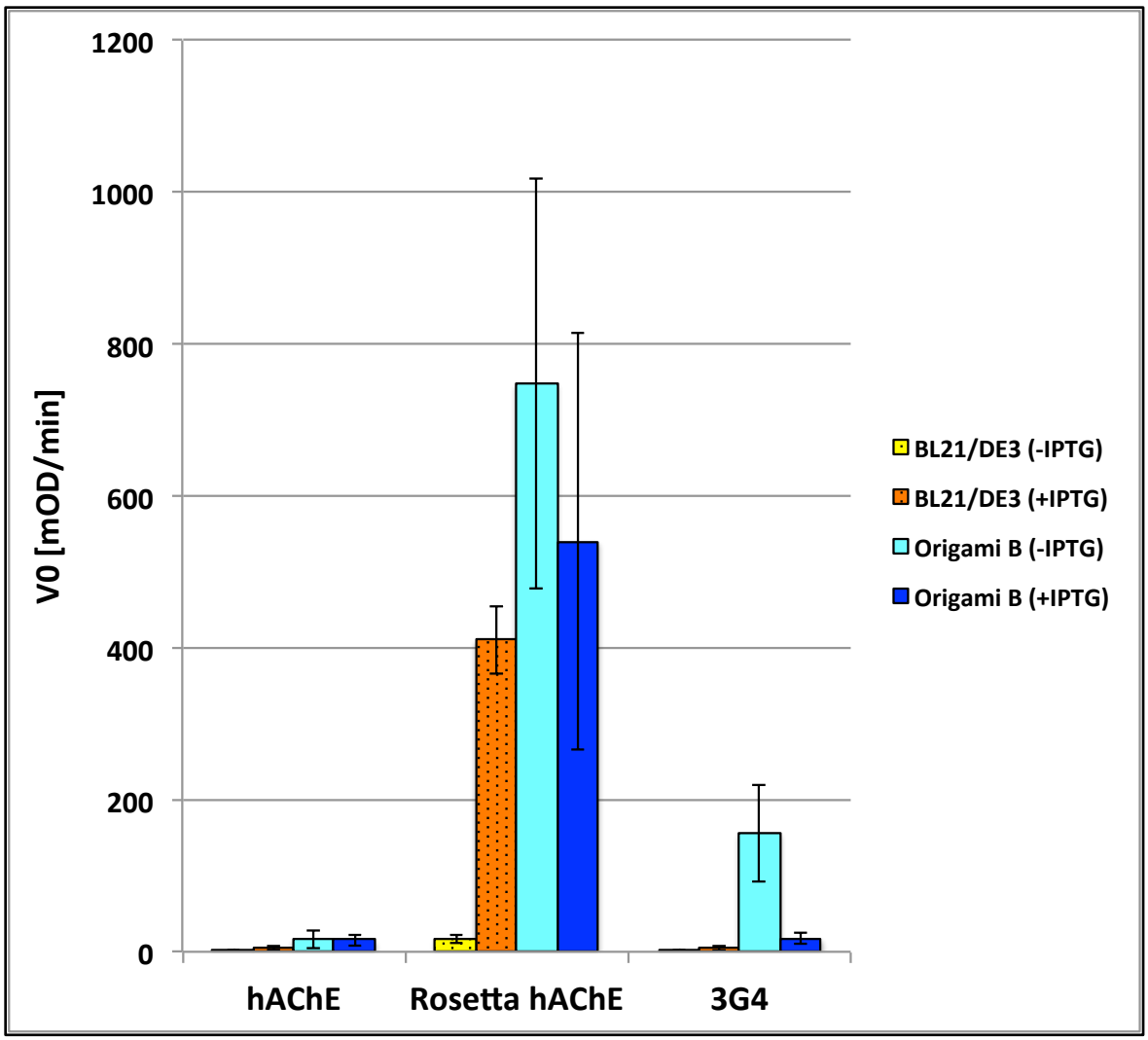

Fig. 16. **Acetylcholinesterase activity in cell lysates of hAChE variants expressed in BL21/DE3 or Origami B strains with or without induction.** Human AChE, its Rosetta designed variant or its ancestral variant 3G4 were expressed in two *E. coli* strains. Single colonies were picked, grown and lysed as described above. AChE hydrolytic activity of clear lysate samples was measured using Ellman's assay and is displayed as average initial velocities (mOD/min) per variant and growth condition. Error bars denote the standard deviations for 24 replicates of each sample.

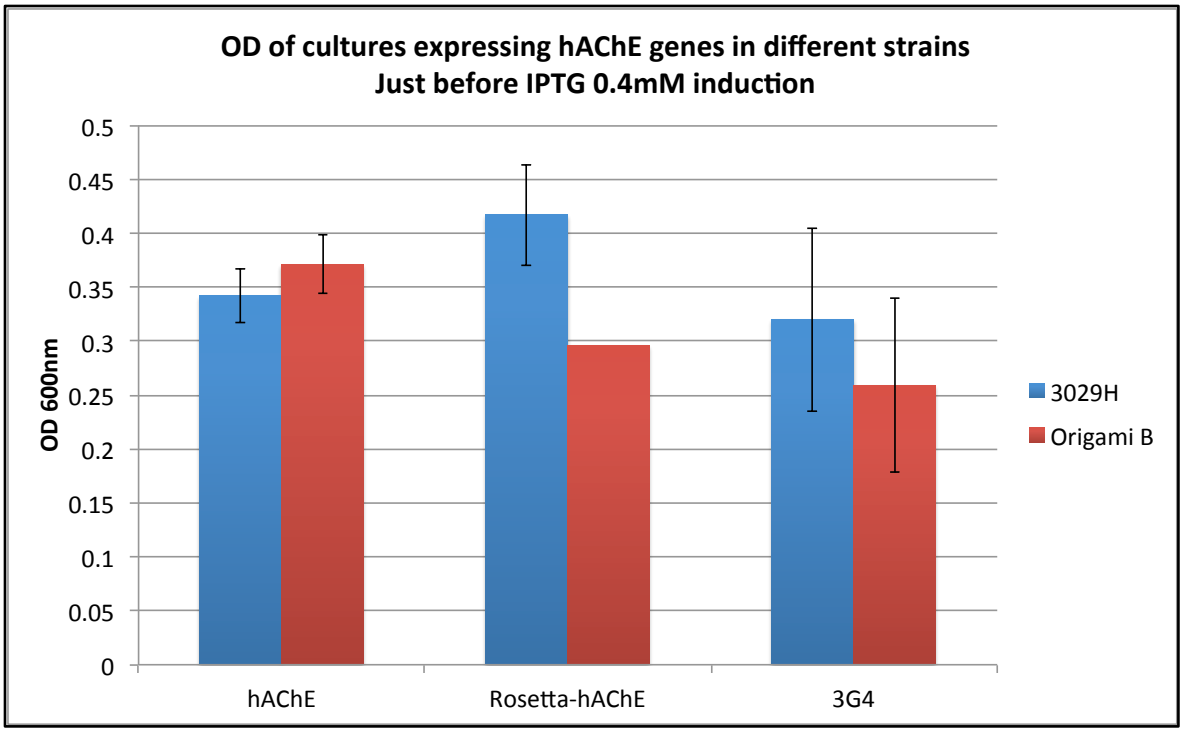

Fig. 17. OD values obtained for *E. coli* cultures expressing different hAChE variants before induction of expression with IPTG.

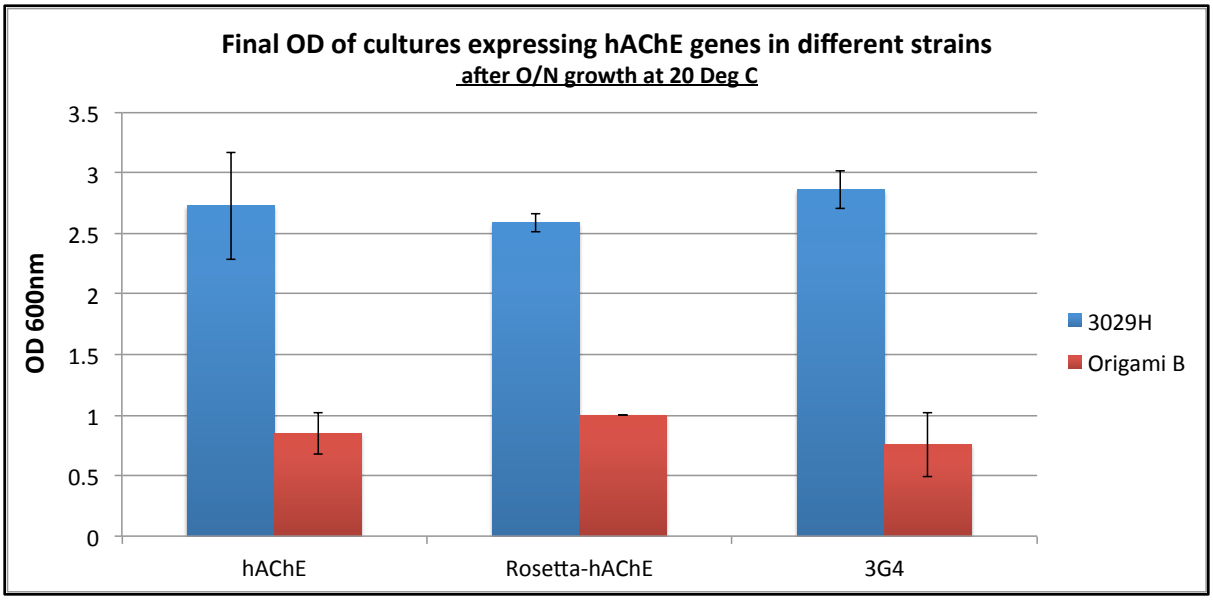

Fig. 18. OD of *E. coli* cultures expressing different hAChE variants after induction with IPTG (0.4mM) and overnight growth at 20°C.

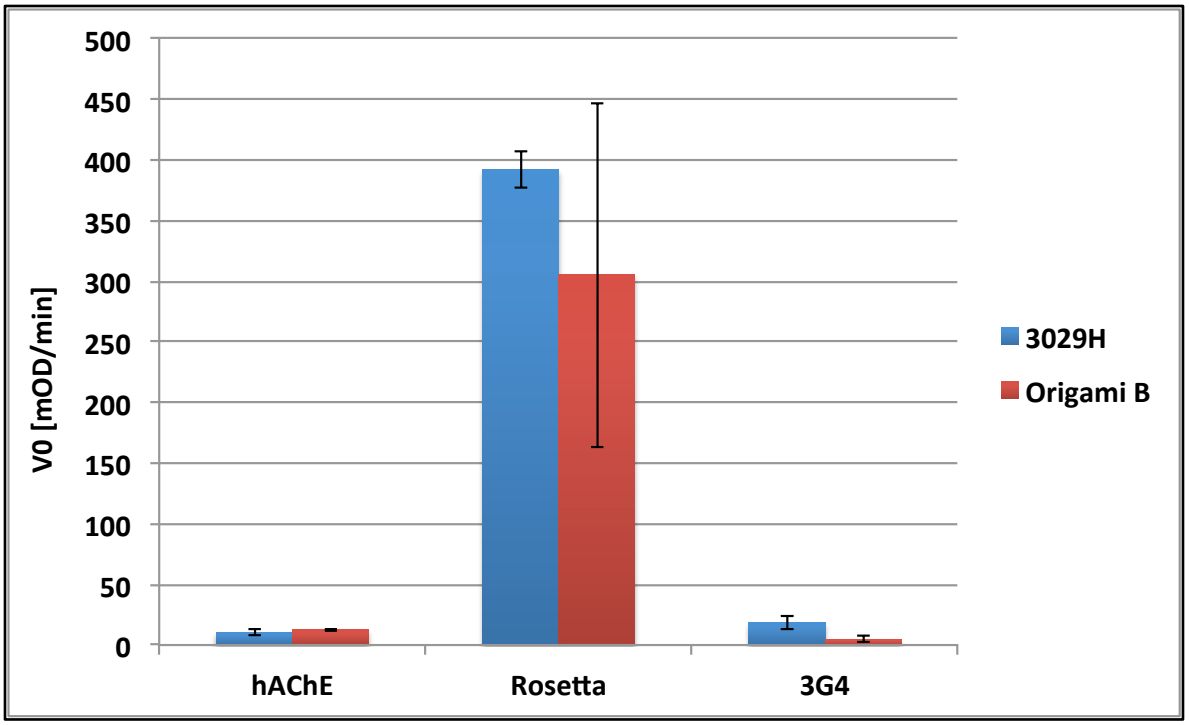

Fig. 19. Rate of acetylthiocholine hydrolysis in cell lysates. Initial rates of acetylthiocholine hydrolysis (V_0) are plotted for each hAChE variant, and for the strain in which it was expressed. Error bars denote the standard deviation derived from duplicate measurements of each of the two cell culture lysates per strain and variant.